

Towards Overcoming False Positives in Visual Relationship Detection

Daisheng Jin^{1,2*}, Xiao Ma^{3*}, Chongzhi Zhang^{1,2*}, Yizhuo Zhou⁴, Jiashu Tao³,
Mingyuan Zhang^{1†}, Haiyu Zhao¹, Shuai Yi¹, Zhoujun Li², Xianglong Liu², Hongsheng Li⁵

¹ SenseTime Research, ² Beihang University, ³ National University of Singapore
⁴ ByteDance AI Lab, ⁵ Multimedia Laboratory, The Chinese University of Hong Kong

Abstract

In this paper, we investigate the cause of the high false positive rate in Visual Relationship Detection (VRD). We observe that during training, the relationship proposal distribution is highly imbalanced: most of the negative relationship proposals are easy to identify, e.g., the inaccurate object detection, which leads to the under-fitting of low-frequency difficult proposals. This paper presents Spatially-Aware Balanced negative pProposal sAmpling (SABRA), a robust VRD framework that alleviates the influence of false positives. To effectively optimize the model under imbalanced distribution, SABRA adopts Balanced Negative Proposal Sampling (BNPS) strategy for mini-batch sampling. BNPS divides proposals into 5 well defined sub-classes and generates a balanced training distribution according to the inverse frequency. BNPS gives an easier optimization landscape and significantly reduces the number of false positives. To further resolve the low-frequency challenging false positive proposals with high spatial ambiguity, we improve the spatial modeling ability of SABRA on two aspects: a simple and efficient multi-head heterogeneous graph attention network (MH-GAT) that models the global spatial interactions of objects, and a spatial mask decoder that learns the local spatial configuration. SABRA outperforms SOTA methods by a large margin on two human-object interaction (HOI) datasets and one general VRD dataset.

1. Introduction

Visual Relationship Detection (VRD) is an important visual task that bridges the gap between middle-level visual perception, e.g., object detection, and high-level visual understanding, e.g., image captioning [42, 9], and visual question answering [31]. General VRD aims to understand the interaction between two arbitrary objects in the

scene. Human-Object Interaction (HOI), as a specific case of VRD, focuses on understanding the interaction between humans and objects, e.g., woman-cut-cake.

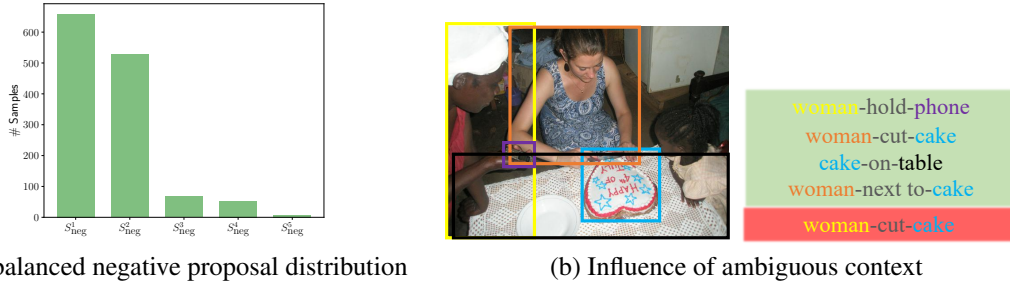
Existing VRD methods focus on building powerful feature extractors for each $[subject, object]$ pair, predicting the *predicate* between the *subject* and the *object*, and outputting $[subject, predicate, object]$ triplet predictions. Some prior works model subject and object relationship independently [8, 35], which loses the global context and is susceptible to inaccurate detections. Some recent works incorporate the union bounding boxes of the $[subject, object]$ as additional features to provide additional spatial information [34, 43] or use the graph neural networks (GNNs) to better extract global object relationships [52, 18, 33]. However, for any visual relationship detector, 90% of its predictions are false positives because according to our statistical result, an image normally contains less than 10 positive relationships, while detectors consider the top-100 predictions.

In addition to the high spatial ambiguity that prior works have been focusing on, we observe that another critical reason for the high false positive rate in VRD is the difficult optimization landscape caused by extremely imbalanced relationship proposal distribution [36]. A typical visual relationship detector takes as input a set of $[subject, object]$ proposals. However, most of them are negative proposals, i.e., no relationship exists for given $[subject, object]$ pairs. We observe that the negative proposals are introduced mainly by two sources with different levels of difficulties: inaccurate single object detections and the incorrect $[subject, object]$ associations. Inaccurate detections, which contribute to more than 90% of the negative proposals (first two columns in Fig. 1.a), can be easily identified by the appearance feature of the single object detections. Incorrect associations contribute to less than 10% of negative proposals (last three columns in Fig. 1.a) but are significantly more difficult: the subject might be related to other objects, but the selected $[subject, object]$ pair can be unrelated, which requires careful inspection of the global context.

We present *Spatially-Aware Balanced negative pProposal*

*Equal contribution

†Corresponding author, zhangmingyuan@sensetime.com



(a) Imbalanced negative proposal distribution

(b) Influence of ambiguous context

Figure 1. (a) VRD normally gives an extremely imbalanced negative proposal distribution, where $S_{\text{neg}}^{1:5}$ denotes 5 different types of negative proposals. Detailed definition of $S_{\text{neg}}^{1:5}$ is given by Eqn. 6. (b) Contextual objects introduce ambiguous information to the relationship classification, e.g., the model thinks the woman on the left is cutting the cake by mistake.

sAmpling (SABRA), a robust and general VRD framework that alleviates the influence of false positives for both HOI and general VRD tasks. According to the two sources of negative proposals, *i.e.*, inaccurate detections, and incorrect associations, we introduce a division of negative proposals into 5 sub-classes $S_{\text{neg}}^{1:5}$. For each single object detection, we consider (1) if it is an accurate detection, and (2) if it is in any relationship with a different object. Specifically, $S_{\text{neg}}^{1:2}$ cover the inaccurate detections, and $S_{\text{neg}}^{3:5}$ discuss the incorrect associations. From S_{neg}^1 to S_{neg}^5 , the sample size decreases, and the classification difficulty increases, because detecting the false positives according to the accuracy of detection is no longer sufficient, and careful understanding about object relationships becomes necessary for the task. Detailed definitions can be found in Eqn. 6. As visualized in Fig. 1.a, the sample sizes of 5 negative proposal sub-classes give a highly imbalanced distribution, which degrades the performance of data-driven VRD algorithms. Inspired by the learning under imbalanced distribution literature [47, 3], we alleviate the optimization difficulty by *Balanced Negative Proposal Sampling* scheme. BNPS computes the statistics of each class and performs a simple yet effective *Class Balanced Sampling* [38] for balanced data distribution. Balanced negative proposal sampling significantly reduces the number of false positive occurrences. For low-frequency difficult classes $S_{\text{neg}}^{3:5}$, e.g., Fig. 1.b, we further improve the spatial modeling of SABRA on two aspects. For the global context understanding, SABRA extends the existing GNN-based methods [50, 33] with a heterogeneous message passing scheme which effectively addresses the distribution divergence between different features. For local spatial configuration, SABRA learns a position-aware embedding vector by predicting the locations in each *[subject, object]* pair.

In our experiment, we evaluate SABRA on two commonly used HOI datasets, V-COCO, and HICO-DET, and one general object relationship detection dataset, VRD. We show that SABRA significantly outperforms SOTA methods by a large margin. We also visualize the results and show that SABRA effectively reduces the false positives in

VRD and misclassification in terms of the spatial ambiguity.

2. Related Works

2.1. Visual Relationship Detection

VRD is an important middle-level task bridging low-level visual recognition with high-level visual understanding. Earlier works focus on *Support Vector Machines* (SVMs) with discriminative features for relationship classification [6, 7]. However, handcrafting features is difficult and harmful to the final performance of VRD algorithms. With the advances of deep learning, data-driven approaches are widely adopted for VRD. Specifically, *Convolutional Neural Networks* (CNNs) are used for automatic feature extraction and information fusion, which achieved great improvement in VRD [43, 49, 46]. *Graph Neural Networks* (GNNs) further improve the feature extraction process by explicitly modeling the instance-wise interactions between objects [50, 33]. Due to the nature of VRD tasks, additional information has been introduced as auxiliary training signals, such as language priors [29], prior interactivity knowledge of objects [23], and action co-occurrence knowledge [22]. In comparison with the existing methods, SABRA is the first to identify the importance of false positives in VRD tasks and has significantly outperformed SOTA methods in our experiments.

2.2. Learning under Imbalanced Distribution

Real-world data is imbalanced by nature: a few high-frequency classes contribute to most of the samples, while a large number of low-frequency classes are under-represented in data. Standard imbalanced learning techniques include data re-balancing [1, 2, 3], loss function engineering [4, 16] and meta-learning [20]. VRD, as a common computer vision task, also suffers from the imbalanced problem [27, 22]. Specifically, [22] considers the imbalance of relationship imbalance, *i.e.*, the imbalance of positive samples, and uses action co-occurrence to provide additional labels. However, none of the existing methods consider the imbalance of the negative *[subject, object]* pro-

posals, which commonly exists in VRD settings. By rebalancing the proposals, SABRA significantly improves the overall performance of VRD algorithms.

2.3. Spatial Information

Spatial information is key to understanding the relationship between objects, e.g., “woman sitting on the chair”. Prior methods fuse spatial information with positional embedding, which normalizes the absolute or relative coordinates of the subject, object, and union bounding boxes [57]. However, simple positional embedding implicitly captures spatial information with position coordinates as inputs to networks, which is unable to capture the explicit spatial configuration in the feature space. [13] introduces binary masks which explicitly specify the subject and object positions, implicitly specifying the spatial configuration by concatenating with union features. With the recent advances in graph neural networks, the relevant positional information can be captured by message passing between instances [59]. The implicit message passing, nevertheless, loses the contextual grounding of the $[subject, object]$ pair. In contrast, the spatial mask decoder learns to predict the positional information of the $[subject, object]$, while capturing the relevant features by end-to-end learning.

3. SABRA

We introduce Spatially-Aware Balanced negative pProposal sAmpling (SABRA) framework for effective visual relationship detection against false positives. The SABRA framework is shown in Fig. 2. SABRA simplifies the difficult optimization landscape of VRD tasks caused by imbalanced proposal distribution by Balanced Negative Proposal Sampling (BNPS) scheme. BNPS divides the imbalanced negative proposals into sub-classes and creates balanced batches for model optimization. In addition, SABRA further improves the existing GNN-based spatial feature extraction pipeline from two perspectives: (1) a heterogeneous message passing scheme for global scene understanding; (2) a spatial mask decoder for local spatial configuration learning. SABRA combines these objectives and achieves the SOTA performance on multiple datasets.

3.1. Balanced Negative Proposal Sampling

3.1.1 Negative Relationship Proposals

Despite abundant researches in improving feature extraction for positive $[subject, predicate, object]$ pairs in VRD, effective learning under a large number of negative proposals is never explored, which has a greater impact on the performance of the VRD task.

Suppose we acquire two sets of bounding boxes $B_{subject}$, B_{object} from the object detector, where $B_{subject}$ contains all the bounding boxes for subjects, and B_{object} con-

tains all the bounding boxes which probably contain an object. A relationship proposal is defined as a tuple (b_1, b_2) . We define the set of relationship proposals S as follows:

$$S = \{(b_1, b_2) \mid b_1 \in B_{subject}, b_2 \in B_{object}\}. \quad (1)$$

S can be divided into two disjoint subsets S_{pos} and S_{neg} ,

$$S = S_{pos} \cup S_{neg}, \quad S_{pos} \cap S_{neg} = \emptyset, \quad (2)$$

where S_{pos} denotes the set of positive proposals that correspond to the ground truth, and S_{neg} stands for the set of wrong proposals, i.e., negative proposals. Specifically,

$$S_{pos} = \{(b_1, b_2) \mid \exists (g_1, g_2) \in GT_{asso}, \min(\text{IoU}(b_1, g_1), \text{IoU}(b_2, g_2)) \geq 0.5\}, \quad (3)$$

where GT_{asso} is the set of ground truth $[subject, object]$ pairs and IoU stands for the intersection of the union.

Given that common VRD algorithms choose top- K detections with highest confidence to generate relationship proposals, we have $|S| = K^2$. However, consider that there are normally less than 10 positive proposals for an image, i.e., $|S_{pos}| < 10$, when $K = 100$, $|S_{pos}|/|S| < 10^{-3}$. Learning under such an extremely imbalanced data distribution is naturally difficult.

One commonly used VRD mini-batch sampling strategy [28], inspired by object detection, is to sample 25% of the mini-batch from S_{pos} and construct the rest 75% by S_{neg} . Although it ensures the presence of positive proposals, it overlooks the complex distribution of negative proposals S_{neg} . Different from object detection, negative proposals in VRD are caused mainly by two reasons: inaccurate detections and incorrect associations. Inaccurate detections cause negative proposals by generating inaccurate bounding boxes with $\text{IoU}(b_1, g_1) < 0.5$. This type of negative proposals can be easily identified by the visual appearance feature of single object detections alone. On the other hand, incorrect associations cause negative proposals in a more complicated way. Due to the limited number of accurate detections D_{pos} , proposals which consist of both correct detections from D_{pos} only contribute a small portion of S . For detections with at least one positive relationship, $D_{rel} = \{b \mid \exists b', (b, b') \in S_{pos} \vee (b', b) \in S_{pos}\}$, we have $|D_{rel}|/|D_{pos}| < 0.2$. Moreover, consider a proposal (b_1, b_2) where $b_1 \in D_{rel}$, i.e., $\exists b'_2, (b_1, b'_2) \in S_{pos}$. The relationship prediction of (b_1, b_2) will be influenced by the positive proposal (b_1, b'_2) , which introduces extra confusion. Thus, the proposals with bounding boxes from D_{rel} are not only under-represented but more confusing. In summary, an imbalanced proposal distribution, where the difficulty of each proposal is negatively correlated with its population size, commonly exists in VRD tasks and would degrade the overall performance of VRD algorithms.

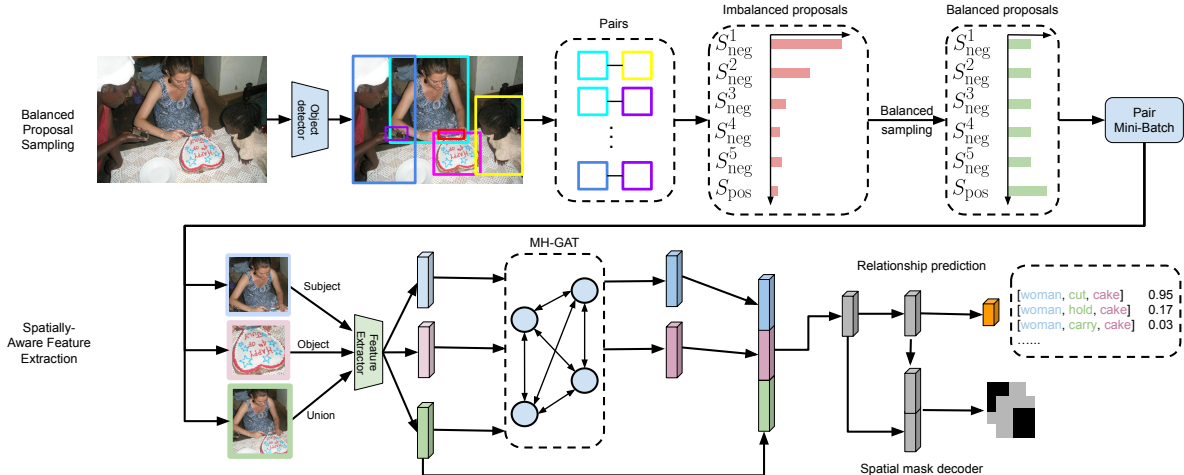


Figure 2. SABRA classifies the false positive [subject, object] proposals into 5 sub-categories $S_{neg}^{1:5}$ and use Balanced-Sampling to re-balance the categorical distribution $\text{Cat}(S_{pos}, S_{neg}^{1:5})$. To reduce the false positive relationship predictions caused by spatial ambiguity, SABRA first uses MH-GAT to capture the global context and then learns to predict the mask of [subject, object].

3.1.2 Balanced Negative Proposal Sampling

Our solution is motivated by learning with data imbalance [1, 2]. We propose a balanced negative proposal sampling strategy considering 1 positive class and 5 negative classes. We first define two helper functions, f_{box} and f_{rel} :

$$f_{\text{box}}(b) = \begin{cases} 1, & \text{if } \exists g \in \text{GT}_{\text{box}}, \text{IoU}(b, g) \geq 0.5, \\ 0, & \text{otherwise.} \end{cases} \quad (4)$$

$$f_{\text{rel}}(b) = \begin{cases} 1, & \text{if } \exists (g_1, g_2) \in \text{GT}_{\text{rel}}, \max \text{IoU}(b, (g_1, g_2)) \geq 0.5, \\ 0, & \text{otherwise,} \end{cases} \quad (5)$$

where GT_{box} denotes the set of ground truth bounding boxes, GT_{rel} denotes the set of ground truth relationships, and $\max \text{IoU}(b, (g_1, g_2)) = \max(\text{IoU}(b, g_1), \text{IoU}(b, g_2))$. Intuitively, $f_{\text{box}}(b)$ indicates if a bounding box b is a positive bounding box, and $f_{\text{rel}}(b)$ denotes if bounding box b belongs to a positive relationship. Next, we divide S_{neg} following these two principles: (1) simple proposals are caused by inaccurate bounding boxes; (2) difficult proposals are introduced by incorrect [subject, object] associations. We formulate the 5 sub-classes:

$$\begin{aligned} S_{\text{neg}}^1 &= \{(b_1, b_2) | \neg f_{\text{box}}(b_1) \wedge \neg f_{\text{box}}(b_2)\}, \\ S_{\text{neg}}^2 &= \{(b_1, b_2) | (\neg f_{\text{box}}(b_1) \wedge f_{\text{box}}(b_2)) \\ &\quad \vee (f_{\text{box}}(b_1) \wedge \neg f_{\text{box}}(b_2))\}, \\ S_{\text{neg}}^3 &= \{(b_1, b_2) | f_{\text{box}}(b_1) \wedge \neg f_{\text{rel}}(b_1) \wedge f_{\text{box}}(b_2) \wedge \neg f_{\text{rel}}(b_2)\}, \\ S_{\text{neg}}^4 &= \{(b_1, b_2) | (f_{\text{rel}}(b_1) \wedge f_{\text{box}}(b_2) \wedge \neg f_{\text{rel}}(b_2)) \vee \\ &\quad (f_{\text{box}}(b_1) \wedge \neg f_{\text{rel}}(b_1) \wedge f_{\text{rel}}(b_2))\}, \\ S_{\text{neg}}^5 &= \{(b_1, b_2) | f_{\text{rel}}(b_1) \wedge f_{\text{rel}}(b_2) \wedge (b_1, b_2) \notin S_{\text{pos}}\}. \end{aligned} \quad (6)$$

This divides the negative proposals into 5 sub-classes: (1) both detections are incorrect; (2) one detection is incorrect; (3) both detections are correct, but they belong to no [subject, predicate, object] triplet; (4) both detections are correct, but only one of them appears in [subject, predicate, object] triplets; (5) both detections are correct, but they appear in two disjoint sets of [subject, predicate, object] triplets, which is the minority of the negative proposals but is the most difficult to learn. Together with the S_{pos} , we divide S into 6 classes, $S = \bigcup_{i=1}^5 S_{\text{neg}}^i \cup S_{\text{pos}}$, which better describe the underlying distribution.

We adopt the most standard *Balanced Sampling* scheme [38] in learning with imbalance literature to address the imbalance of negative proposals S_{neg} , and we introduce Balanced Negative Proposal Sampling (BNPS). During training time, for each image, we find the top- K object detections, construct $K \times K$ relationship proposals, and count the number of samples for each class. For each proposal s_i , we assign a weight w_i :

$$w_i = \begin{cases} 0.25/|S_{\text{pos}}|, & \text{if } s_i \in S_{\text{pos}}, \\ 0.15/|S_{\text{neg}}^j|, & \text{if } s_i \in S_{\text{neg}}^j, j = 1, \dots, 5 \end{cases} \quad (7)$$

where we keep the weight, 0.25, of positive proposals, while re-balancing the weight of negative proposals, which improves the prediction of low-frequency difficult classes.

3.2. Spatially-Aware Embedding Learning

For low-frequency difficult false positives, GNNs generally improve the global scene understanding [50, 33, 23] and learning the spatial position of objects improves the local feature representation of [subject, object] pairs [57, 24,

59]. For global features, SABRA improves the graph representation learning in VRD by Multi-head Heterogeneous Graph Attention networks (MH-GAT) for message passing. For local features, SABRA uses a Spatial Mask Decoder (SMD) to explicitly model the positional configuration of a $[subject, object]$ pair.

3.2.1 Multi-head Heterogeneous Graph Attention

We introduce Multi-head Heterogeneous Graph Attention Networks (MH-GAT) for effective learning of the global context. One limitation of widely used Graph Attention networks is that it assumes a homogeneous node feature distribution and uses the same set of parameters for learning embeddings for all nodes [41]. However, the features of subjects, objects, and union bounding boxes often follow different distributions. Directly using GAT might degrade the final performance. MH-GAT extends GAT by performing message passing on heterogeneous nodes, i.e., subject, object, and union feature, in VRD. We treat each object in the image as a node i with feature x_i , and construct a fully connected graph $G = (V, E)$, where $|V| = N$ is the set of nodes and $E = \{(i, j) \mid i, j = 1, 2, \dots, N\}$. We treat the feature for edge (i, j) as the union feature e_{ij} . The MH-GAT message passing mechanism is as follows:

$$x'_i = x_i + \sum_{j \in N(i) \cup \{i\}} \alpha_{ij} f_m([x_i, x_j, e_{ij}]), \quad (8)$$

$$\alpha_{ij} = \frac{\exp(g_{ij})}{\sum_{k \in N(i) \cup \{i\}} \exp(g_{ik})}, \quad (9)$$

$$g_{ij} = [f_s(x_i), f_t(x_j), f_e(e_{ij})], \quad (10)$$

where α_{ij} is the attention weight for edge (i, j) , f_m , f_s , f_t and f_e are functions for message embedding, source node feature embedding, target node feature embedding, and edge feature embedding respectively. In contrast to most of the GNNs, when computing the attention values, we process source features, target features, edge features with different functions. This allows modeling the heterogeneous distribution between different nodes. This formulation also enables our model to pass diverse features from a single source node to different target nodes. Besides, we apply a multi-head attention mechanism, which provides a better modeling ability to capture the complex attentions among objects.

3.2.2 Spatial Mask Decoder

To learn the local spatial configuration, we present Spatial Mask Decoder (SMD) which predicts the locations of $[subject, object]$. The architecture of SMD is given in Fig. 3. SMD predicts a $2 \times l_p \times l_p$ mask using the VRD feature vectors, where l_p represents the pooling size and the two chan-

nels represent the spatial location of subjects and objects in the pooled feature map with size l_p . This guarantees that the local spatial configuration is tightly embedded in the feature vector for relationship prediction. We scale the absolute coordinates of the $[subject, object]$ pair to get the relative position in the pooled feature map. Compared to reconstruction in the image space, the ROI feature space preserves the locality of the union bounding box but requires fewer parameters. Different from the standard positional embedding [57] which implicitly utilizes the spatial information with the absolute positions as an input, SMD explicitly learns a structured embedding. Compared to [13] which concatenates binary mask as position feature, SMD explicitly imposes the spatial structure in the embedding vector and gives better spatially-aware embeddings. We empirically show SMD outperforms these variants in our experiments.

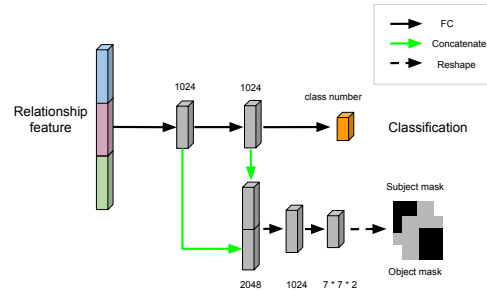


Figure 3. Structure of Spatial Mask Decoder

3.3. SABRA Framework

The pipeline of SABRA is shown in Fig. 2. The input image is fed into an object detector to predict all bounding boxes, which are exhaustively paired to generate all relationship proposals. In the proposal sampling stage, given the imbalanced relationship proposals, SABRA constructs a balanced pair mini-batch by BNPS that samples data point i proportionally to its weight w_i . The features of subjects, objects, and union bounding boxes are fed into MH-GAT with heterogeneous message passing to extract spatial object interactions. We use only one layer of MH-GAT to avoid over-smoothing in GNNs [54]. The mask decoder discovers the spatial configuration of $[subject, object]$ pairs in the learned embeddings. SABRA is robust to the imbalanced negative proposal distribution and reduces the number of false positive predictions caused by spatial ambiguity. More details are available in the appendix.

During training, we jointly optimize the object detector and relationship classifier by

$$L = L_{RPN}^{cls} + L_{RPN}^{loc} + L_{RCNN}^{cls} + L_{RCNN}^{loc} + L_{VRD}^{cls} + L_{VRD}^{mask}, \quad (11)$$

where L_{RPN}^{cls} , L_{RPN}^{loc} , L_{RCNN}^{cls} , L_{RCNN}^{loc} are losses for object detection. Their definitions are the same as [37]. L_{VRD}^{cls} is a classification loss of each relation proposal. L_{VRD}^{mask} is an

| Method | Backbone | V-COCO | | HICO-DET | | | | |
|---------------------------|--------------|--------------|--------------|--------------|--------------|---------------|--------------|--------------|
| | | AP_{role} | Default | | | Known Objects | | |
| | | | Full | Rare | Non-Rare | Full | Rare | Non-Rare |
| iCAN [11] | ResNet50 | 45.30 | 14.84 | 10.45 | 16.15 | 16.26 | 11.33 | 17.73 |
| Contextual Attention [45] | ResNet50 | 47.30 | 16.24 | 11.16 | 17.75 | 17.73 | 12.78 | 19.21 |
| In-GraphNet [51] | ResNet50 | 48.90 | 17.72 | 12.93 | 13.91 | - | - | - |
| VCL [17] | ResNet50 | 48.30 | 19.43 | 16.55 | 20.29 | 22.00 | 19.09 | 22.87 |
| PD-Net [58] | ResNet50 | 52.30 | 20.76 | 15.68 | 22.28 | 25.58 | 19.93 | 27.28 |
| SABRA(Ours) | ResNet50 | 53.57 | 23.48 | 16.39 | 25.59 | 28.79 | 22.75 | 30.54 |
| InteractNet [14] | ResNet50-FPN | 40.00 | 9.94 | 7.16 | 10.77 | - | - | - |
| PMFNet [43] | ResNet50-FPN | 52.00 | 17.46 | 15.65 | 18.00 | 20.34 | 17.47 | 21.20 |
| DRG [10] | ResNet50-FPN | 51.00 | 19.26 | 17.74 | 19.71 | 23.40 | 21.75 | 23.89 |
| IP-Net [46] | ResNet50-FPN | 51.00 | 19.56 | 12.79 | 21.58 | 22.05 | 15.77 | 23.92 |
| Contextual HGNN [44] | ResNet50-FPN | 52.70 | 17.57 | 16.85 | 17.78 | 21.00 | 20.74 | 21.08 |
| SABRA(Ours) | ResNet50-FPN | 54.69 | 24.12 | 15.91 | 26.57 | 29.65 | 22.92 | 31.65 |
| VSGNet [40] | ResNet152 | 51.76 | 19.80 | 16.05 | 20.91 | - | - | - |
| PD-Net [58] | ResNet152 | 52.20 | 22.37 | 17.61 | 23.79 | 26.89 | 21.70 | 28.44 |
| ACP [21] | ResNet152 | 52.98 | 20.59 | 15.92 | 21.98 | - | - | - |
| SABRA(Ours) | ResNet152 | 56.62 | 26.09 | 16.29 | 29.02 | 31.08 | 23.44 | 33.37 |

Table 1. Results on V-COCO and HICO-DET datasets. In most of the cases, SABRA significantly outperforms SOTA methods.

| Method | Backbone | Relationship Detection | | | | Phrase Detection | | | |
|----------------------|-----------------|------------------------|--------------|--------------|--------------|------------------|--------------|--------------|--------------|
| | | k=1 | | k=70 | | k=1 | | k=70 | |
| | | R@50 | R@100 | R@50 | R@100 | R@50 | R@100 | R@50 | R@100 |
| VRD [30] | VGG16 | 17.03 | 16.17 | 24.90 | 20.04 | 14.70 | 13.86 | 21.51 | 17.35 |
| KL distillation [55] | VGG16 | 19.17 | 21.34 | 22.68 | 31.89 | 23.14 | 24.03 | 26.32 | 29.43 |
| Zoom-Net [53] | VGG16 | 18.92 | 21.41 | 21.37 | 27.30 | 24.82 | 28.09 | 29.05 | 37.34 |
| CAI + SCA-M [53] | VGG16 | 19.54 | 22.39 | 22.34 | 28.52 | 25.21 | 28.89 | 29.64 | 38.39 |
| Hose-Net [48] | VGG16 | 20.46 | 23.57 | 22.13 | 27.36 | 27.04 | 31.71 | 28.89 | 36.16 |
| ReIDN [57] | VGG16 | 18.92 | 22.96 | 21.52 | 26.38 | 26.37 | 31.42 | 28.24 | 35.44 |
| AVR [32] | VGG16 | 22.83 | 25.41 | 27.35 | 32.96 | 29.33 | 33.27 | 34.51 | 41.36 |
| SABRA(Ours) | VGG16 | 24.47 | 29.16 | 27.27 | 33.99 | 30.57 | 36.80 | 33.39 | 41.79 |
| GPS-Net [28] | VGG16 (MS COCO) | 21.50 | 24.30 | - | - | 28.90 | 34.00 | - | - |
| MCN [56] | VGG16 (MS COCO) | 24.50 | 28.00 | - | - | 31.80 | 37.10 | - | - |
| SABRA(Ours) | VGG16 (MS COCO) | 26.29 | 31.08 | 29.44 | 36.44 | 32.01 | 38.48 | 35.45 | 44.07 |
| UVTransE [19] | VGG16 (VG) | 25.66 | 29.71 | 27.32 | 34.11 | 30.01 | 36.18 | 31.51 | 39.79 |
| SABRA(Ours) | VGG16 (VG) | 27.87 | 32.48 | 30.71 | 37.71 | 33.56 | 39.62 | 36.62 | 45.29 |
| ATR-Net [12] | ResNet101 | - | - | - | - | 31.96 | 36.54 | 36.06 | 43.45 |
| SABRA(Ours) | ResNet101 | 26.73 | 31.11 | 29.92 | 37.43 | 32.81 | 38.68 | 36.24 | 45.26 |

Table 2. Results on the VRD dataset. SABRA outperforms all SOTA methods by a large margin in all cases. By default, all backbones are pretrained with ImageNet. To align with the setups of some prior works [28, 56, 19], we use MS COCO or Visual Genome as additional data for training, denoted by VGG (MS COCO) or VGG (VG).

auxiliary loss used in our SMD model. These two losses are designed for the VRD branch. We opt for Binary Cross Entropy loss for both items. During inference, SABRA predicts all given relationship proposals without sampling.

4. Experiment

We evaluate SABRA on three commonly used datasets: V-COCO [15], HICO-DET [5], and VRD [30], covering both human-object interaction (V-COCO and HICO-DET) and general object relationship detection (VRD). We compared SABRA over 20 SOTA methods. Specifically, we

trained SABRA with different backbones and perform a comprehensive and fair comparison with existing methods. We incrementally add our proposed components to a baseline model. The baseline directly concatenates appearance features of subjects, objects, and their union features, which are fed into a 3-layer Multi-Layer Perceptron (MLP) for classification.

As a brief conclusion, we show that: 1) SABRA generally outperforms other methods by a large margin; 2) the balanced negative proposal sampling strategy can reduce the number of false positive predictions; 3) spatial mask decoder successfully reduces the number of false positives

| | Sampling | Spatial Learning | GNN | AP_{role} |
|----|-----------|------------------|----------------|--------------|
| 1 | - | - | - | 50.20 |
| 2 | BNPS | - | - | 52.24 |
| 3 | - | SMD | - | 50.84 |
| 4 | - | - | MH-GAT | 51.65 |
| 5 | - | SMD | MH-GAT | 52.82 |
| 6 | BNPS-2cls | SMD | MH-GAT | 53.74 |
| 7 | BNPS-3cls | SMD | MH-GAT | 53.93 |
| 8 | BNPS | - | MH-GAT | 53.67 |
| 9 | BNPS | Binary [13] | MH-GAT | 53.90 |
| 10 | BNPS | PE [57] | MH-GAT | 54.29 |
| 11 | BNPS | SMD | - | 52.53 |
| 12 | BNPS | SMD | M-GAT | 51.65 |
| 13 | BNPS | SMD | MH-GAT-no-edge | 53.80 |
| 14 | BNPS | SMD | MH-GAT | 54.69 |

Table 3. Ablation Study on V-COCO dataset. We compare each model variant with the baseline (row 1) and the SABRA (row 14).

caused by spatial ambiguity.

4.1. Datasets

V-COCO is based on the 80-class object detection annotations of COCO [25]. It has 10,346 images (2,533 for training, 2,867 for validating and 4,946 for testing). HICO-DET has a total of 47,774 images, covering 600 categories of human-object interactions over 117 common actions on 80 common objects. VRD dataset contains 4,000 images in the train split and 1,000 in the test split. It has 100 different types of objects and 70 types of relationships.

4.2. Evaluation Metrics

We followed the convention in prior literature and used three different evaluation metrics for these datasets.

Following [30], we use Recall@ N as our evaluation metric on VRD. Recall@ N computes the *recall* rates using the top N predictions per image. To be consistent with prior works, we report Recall@50 and Recall@100 in our experiments. We evaluate two tasks: *relationship detection* that outputs triple labels and evaluates bounding boxes of the subject and object separately; *phrase recognition* that takes a triplet as a union bounding box and predicts the triple labels. Besides, we report the top- k predictions as [55], where $k = 1$ or $k = 70$.

For V-COCO and HICO-DET, mean average precision (mAP) is used to estimate the performance. A triplet [human, verb, object] is considered a positive prediction if and only if there exists a triplet [human', verb', object'] in the ground truth satisfying: (1) $\text{IoU}(\text{human}, \text{human}') \geq 0.5$, (2) $\text{verb} = \text{verb}'$, (3) $\text{IoU}(\text{object}, \text{object}') \geq 0.5$

In HICO-DET, we calculate the mAP among all pairs of [verb, object]. In *Default* mode, we calculate AP on all images. In *Known Objects* mode, the category of the bounding box is known and we only calculate AP between humans

and objects from a specific category. In V-COCO, we calculate the mAP for all categories of verbs, which is called AP_{role} . More details are available in the appendix.

4.3. Quantitative Results

We present our results in Table 1 for HOI datasets (V-COCO and HICO-DET) and Table 2 for the VRD dataset. For HOI, we cluster our results according to the backbones, including ResNet50, ResNet50-FPN, and ResNet152, with increasing feature extraction ability. For VRD datasets, VGG-16 pretrained on ImageNet is used for all methods. To align with the setup of some prior works [28, 56, 19], we use MS COCO and VG as additional datasets for VGG16.

We observe that SABRA generally improves the SOTA methods significantly on all datasets for both HOI and VRD. For example, on V-COCO with ResNet152 backbone, SABRA achieves 56.62 mAP while the SOTA model, ACP [22] gives an mAP of 52.98. Specifically, we want to highlight the performance gain of SABRA on the V-COCO dataset. V-COCO uses the object annotations of the COCO dataset, which are accurate and include all objects, regardless of the relationships. This gives a more imbalanced distribution than HICO-DET, where only the objects in relationships are considered. Furthermore, accurate annotations also give rise to better object detection, which amplifies the significance of spatial information for a good performance. Specifically, we noticed that for PD-Net [58], using a more powerful backbone (ResNet152) gives no performance gain than the smaller one (ResNet50). SABRA, on the contrary, can fully exploit the feature extraction power of ResNet152 and give a large performance improvement compared with ResNet50 (56.62 V.S. 53.57).

4.4. Ablation Studies

We conduct a comprehensive ablation study on the V-COCO dataset to understand each proposed component: Balanced Negative Proposal Sampling (BNPS), Multi-head Heterogeneous Graph Attention (MH-GAT), and Spatial Mask Decoder (SMD). We present the results in Table 3, where row 1 denotes the baseline model and row 14 denotes SABRA with all proposed components.

Each proposed component improves the baseline. We perform incremental analysis in rows 1-4. Specifically, we observe that by simply improving the optimization process with BNPS, baseline + BNPS (row 2) gains 2.04 improvement on AP_{role} . This suggests that imbalanced proposal distribution significantly hinders the model performance, and BNPS addresses this issue effectively.

Balancing negative proposal distribution generally improves the VRD performance. In rows 5-7 and row 14, we compare BNPS with 3 other alternatives. (1) BNPS-3cls (row 7): balanced sampling over $\{S_{neg}^1, S_{neg}^2, S_{neg}^3 \cup S_{neg}^4 \cup S_{neg}^5\}$, i.e., ignoring the difference between negative pro-



Figure 4. Qualitative analysis of SABRA on V-COCO dataset. (a) The number of false positive predictions under each class by Baseline model, SABRA w/o BNPS, SABRA w/o spatial module (MH-GAT + SMD), and SABRA. BNPS and spatial module significantly reduce the number of false positive predictions. (b) Predictions of SABRA. In sub-predicate-obj(v_1, v_2), v_1 denotes the prediction confidence of the baseline model and v_2 denotes the confidence of SABRA. SABRA successfully reduced the low-frequency difficult false positives.

posals when detections are correct; (2) BNPS-2cls (row 6): balanced sampling over $\{S_{neg}^1 \cup S_{neg}^2, S_{neg}^3 \cup S_{neg}^4 \cup S_{neg}^5\}$, i.e., further ignoring the differences of negative proposals when detections are incorrect; (3) None (row 5): we remove the BNPS. We fix the positive sample rate to be 25% and balance the rest 75% samples over the given distributions. Comparing BNPS with BNPS-2cls and BNPS-3cls, we conclude BNPS improves prediction accuracy for both inaccurate detections and incorrect associations.

Understanding spatial information is crucial to VRD.

In rows 8-10 and row 14, we compare the proposed Spatial Mask Decoder (SMD) with 3 alternatives. (1) Binary (row 9) [13]: a binary mask over the union feature to specify the position of $[subject, object]$; (2) PE (row 10) [57]: naive positional embedding; (3) None (row 8): no spatial learning module. We conclude that: (1) adding spatial information learning generally improves the performance; (2) Implicitly imposing spatial information with PE or binary masks gives worse performance than SMD which enforces an explicit constraint over the feature space.

MH-GAT is more effective in heterogeneous VRD graphs In rows 11-13 and row 14, we compare MH-GAT with other 4 alternatives: (1) Multi-head GAT [41] (row 12), standard homogeneous message passing scheme which has the same number of heads and edge features used in MH-GAT, (2) MH-GAT without edge feature (row 13), and (3) None (row 11). We observe that: (1) GNNs generally improve the VRD performance; (2) by separating the parameters for objects, subjects, and union features, the heterogeneous message passing scheme in MH-GAT improves the M-GAT; (3) edge feature gives extra information and is important to MH-GAT.

4.5. Qualitative Analysis

Qualitatively, we provide extra statistics and visualizations on the V-COCO dataset to better understand the performance improvement of SABRA in Fig. 4.

To verify the ability of SABRA on reducing the number

of false positives, we compute the per-image false positive predictions for $S_{neg}^{1:5}$ by thresholding the prediction confidence at 0.5 in Fig. 4. Compared with the baseline, SABRA w/o BNPS, SABRA w/o Spatial, and SABRA have reduced the total number of low-frequency difficult $S_{neg}^{3:5}$ by 14.7%, 58.5%, and 71.1%. BNPS gave a sharp decrease on $S_{neg}^{3:5}$, which suggests the necessity of learning from a balanced proposal distribution. The spatial module successfully filtered the irrelevant objects in S_{neg}^3 and significantly reduced the number of false positives in total. Combining both of them, SABRA gives the best performance among all alternatives. However, we also noticed that on $S_{neg}^{4:5}$ and $S_{neg}^{1:2}$, the spatial module has no clear improvement, because the spatial module potentially overexploited the correct detection of the positive $[subject, predicate, object]$ triplet. Auxiliary constraints on the relationship assignment could be considered to address this issue. We leave it for future study.

We visualize two examples of SABRA successfully reducing the low-frequency difficult false positives where both detections are correct in Fig. 4.b. Without the spatial module, the VRD algorithm assigns high confidence (0.92) to the $[subject, object]$ pair that the woman is cutting the cake. This confidence was reduced to 0.13 by SABRA.

5. Conclusion

We present SABRA for alleviating false positives in VRD. We divided the negative $[subject, object]$ proposals into 5 sub-classes with imbalanced data distribution, and addressed the data imbalance by Balanced Negative Proposal Sampling. SABRA incorporates the global contextual information with MH-GAT and local spatial configuration by SMD. SABRA significantly outperforms the SOTA methods on V-COCO, HICO-DET, and VRD datasets.

As the first paper to consider the data imbalance in the negative proposal distribution, SABRA used a relatively simple strategy, balanced sampling. More advanced techniques, e.g., Meta-Learning [36], could be considered.

References

- [1] Ricardo Barandela, E Rangel, José Salvador Sánchez, and Francesc J Ferri. Restricted decontamination for the imbalanced training sample problem. In *Iberoamerican congress on pattern recognition*, pages 424–431. Springer, 2003. 2, 4
- [2] Mateusz Buda, Atsuto Maki, and Maciej A Mazurowski. A systematic study of the class imbalance problem in convolutional neural networks. *Neural Networks*, 106:249–259, 2018. 2, 4
- [3] Jonathon Byrd and Zachary Lipton. What is the effect of importance weighting in deep learning? In *International Conference on Machine Learning*, pages 872–881, 2019. 2
- [4] Kaidi Cao, Colin Wei, Adrien Gaidon, Nikos Arachida, and Tengyu Ma. Learning imbalanced datasets with label-distribution-aware margin loss. In *Advances in Neural Information Processing Systems*, pages 1567–1578, 2019. 2
- [5] Yu-Wei Chao, Yunfan Liu, Xieyang Liu, Huayi Zeng, and Jia Deng. Learning to detect human-object interactions. In *2018 IEEE Winter Conference on Applications of Computer Vision, WACV 2018, Lake Tahoe, NV, USA, March 12-15, 2018*. IEEE Computer Society, 2018. 6
- [6] Vincent Delaitre, Ivan Laptev, and Josef Sivic. Recognizing human actions in still images: a study of bag-of-features and part-based representations. In *Proceedings of the British Machine Vision Conference*, 2010. 2
- [7] Vincent Delaitre, Josef Sivic, and Ivan Laptev. Learning person-object interactions for action recognition in still images. In *Advances in neural information processing systems*, pages 1503–1511, 2011. 2
- [8] Carolina Galleguillo, Andrew Rabinovich, and Serge Belongie. Object categorization using co-occurrence, location and appearance. In *2008 IEEE Conference on Computer Vision and Pattern Recognition*, pages 1–8. IEEE, 2008. 1
- [9] Chuang Gan, Zhe Gan, Xiaodong He, Jianfeng Gao, and Li Deng. Stylenet: Generating attractive visual captions with styles. In *Proceedings of the IEEE Conference on Computer Vision and Pattern Recognition*, pages 3137–3146, 2017. 1
- [10] Chen Gao, Jiarui Xu, Yuliang Zou, and Jia-Bin Huang. DRG: dual relation graph for human-object interaction detection. In Andrea Vedaldi, Horst Bischof, Thomas Brox, and Jan-Michael Frahm, editors, *Computer Vision - ECCV 2020 - 16th European Conference, Glasgow, UK, August 23-28, 2020, Proceedings, Part XII*, volume 12357 of *Lecture Notes in Computer Science*, pages 696–712. Springer, 2020. 6
- [11] Chen Gao, Yuliang Zou, and Jia-Bin Huang. ican: Instance-centric attention network for human-object interaction detection. In *British Machine Vision Conference 2018, BMVC 2018, Newcastle, UK, September 3-6, 2018*. BMVA Press, 2018. 6
- [12] Nikolaos Gkanatsios, Vassilis Pitsikalis, Petros Koutras, and Petros Maragos. Attention-translation-relation network for scalable scene graph generation. In *Proceedings of the IEEE International Conference on Computer Vision Workshops*, 2019. 6
- [13] Nikolaos Gkanatsios, Vassilis Pitsikalis, Petros Koutras, Athanasia Zlatintsi, and Petros Maragos. Deeply supervised multimodal attentional translation embeddings for visual relationship detection. In *2019 IEEE International Conference on Image Processing, ICIP 2019, Taipei, Taiwan, September 22-25, 2019*, pages 1840–1844. IEEE, 2019. 3, 5, 7, 8
- [14] Georgia Gkioxari, Ross B. Girshick, Piotr Dollár, and Kaiming He. Detecting and recognizing human-object interactions. In *2018 IEEE Conference on Computer Vision and Pattern Recognition, CVPR 2018, Salt Lake City, UT, USA, June 18-22, 2018*, 2018. 6, 11
- [15] Saurabh Gupta and Jitendra Malik. Visual semantic role labeling. *CoRR*, 2015. 6
- [16] Munawar Hayat, Salman Khan, Syed Waqas Zamir, Jianbing Shen, and Ling Shao. Gaussian affinity for max-margin class imbalanced learning. In *Proceedings of the IEEE International Conference on Computer Vision*, pages 6469–6479, 2019. 2
- [17] Zhi Hou, Xiaojiang Peng, Yu Qiao, and Dacheng Tao. Visual compositional learning for human-object interaction detection. *CoRR*, abs/2007.12407, 2020. 6
- [18] Yue Hu, Siheng Chen, Xu Chen, Ya Zhang, and Xiao Gu. Neural message passing for visual relationship detection. In *ICML Workshop on Learning and Reasoning with Graph-Structured Representations, Long Beach, CA, 2019*. 1
- [19] Zih-Siou Hung, Arun Mallya, and Svetlana Lazebnik. Contextual translation embedding for visual relationship detection and scene graph generation. *IEEE Transactions on Pattern Analysis and Machine Intelligence*, 2020. 6, 7
- [20] Muhammad Abdullah Jamal, Matthew Brown, Ming-Hsuan Yang, Liqiang Wang, and Boqing Gong. Rethinking class-balanced methods for long-tailed visual recognition from a domain adaptation perspective. In *Proceedings of the IEEE/CVF Conference on Computer Vision and Pattern Recognition*, pages 7610–7619, 2020. 2
- [21] Dong-Jin Kim, Xiao Sun, Jinsoo Choi, Stephen Lin, and In So Kweon. Detecting human-object interactions with action co-occurrence priors. *CoRR*, 2020. 6
- [22] Dong-Jin Kim, Xiao Sun, Jinsoo Choi, Stephen Lin, and In So Kweon. Detecting human-object interactions with action co-occurrence priors. *arXiv preprint arXiv:2007.08728*, 2020. 2, 7
- [23] Yong-Lu Li, Siyuan Zhou, Xijie Huang, Liang Xu, Ze Ma, Hao-Shu Fang, Yanfeng Wang, and Cewu Lu. Transferable interactiveness knowledge for human-object interaction detection. In *Proceedings of the IEEE Conference on Computer Vision and Pattern Recognition*, pages 3585–3594, 2019. 2, 4
- [24] Xiaodan Liang, Lisa Lee, and Eric P. Xing. Deep variation-structured reinforcement learning for visual relationship and attribute detection. In *2017 IEEE Conference on Computer Vision and Pattern Recognition, CVPR 2017, Honolulu, HI, USA, July 21-26, 2017*. IEEE Computer Society, 2017. 5
- [25] Tsung-Yi Lin, Michael Maire, Serge J. Belongie, James Hays, Pietro Perona, Deva Ramanan, Piotr Dollár, and C. Lawrence Zitnick. Microsoft COCO: common objects in context. In David J. Fleet, Tomás Pajdla, Bernt Schiele, and Tinne Tuytelaars, editors, *Computer Vision - ECCV 2014 - 13th European Conference, Zurich, Switzerland, September 6-12, 2014, Proceedings, Part V*, 2014. 7

- [26] Tsung-Yi Lin, Priya Goyal, Ross Girshick, Kaiming He, and Piotr Dollar. Focal loss for dense object detection. In *Proceedings of the IEEE International Conference on Computer Vision (ICCV)*, Oct 2017. 13
- [27] Xin Lin, Changxing Ding, Jinqun Zeng, and Dacheng Tao. Gps-net: Graph property sensing network for scene graph generation. In *Proceedings of the IEEE/CVF Conference on Computer Vision and Pattern Recognition*, pages 3746–3753, 2020. 2
- [28] Xin Lin, Changxing Ding, Jinqun Zeng, and Dacheng Tao. Gps-net: Graph property sensing network for scene graph generation. In *2020 IEEE/CVF Conference on Computer Vision and Pattern Recognition, CVPR 2020, Seattle, WA, USA, June 13-19, 2020*. IEEE, 2020. 3, 6, 7
- [29] Cewu Lu, Ranjay Krishna, Michael Bernstein, and Li Fei-Fei. Visual relationship detection with language priors. In *European conference on computer vision*, pages 852–869. Springer, 2016. 2
- [30] Cewu Lu, Ranjay Krishna, Michael S. Bernstein, and Fei-Fei Li. Visual relationship detection with language priors. In *Computer Vision - ECCV 2016 - 14th European Conference, Amsterdam, The Netherlands, October 11-14, 2016, Proceedings, Part I*, 2016. 6, 7
- [31] Jiasen Lu, Jianwei Yang, Dhruv Batra, and Devi Parikh. Hierarchical question-image co-attention for visual question answering. In *Advances in neural information processing systems*, pages 289–297, 2016. 1
- [32] Jianming Lv, Qinzhe Xiao, and Jiajie Zhong. Avr: Attention based salient visual relationship detection. *arXiv preprint arXiv:2003.07012*, 2020. 6
- [33] Li Mi and Zhenzhong Chen. Hierarchical graph attention network for visual relationship detection. In *Proceedings of the IEEE/CVF Conference on Computer Vision and Pattern Recognition*, pages 13886–13895, 2020. 1, 2, 4
- [34] Siyuan Qi, Wenguan Wang, Baoxiong Jia, Jianbing Shen, and Song-Chun Zhu. Learning human-object interactions by graph parsing neural networks. In *Computer Vision - ECCV 2018 - 15th European Conference, Munich, Germany, September 8-14, 2018, Proceedings, Part IX*, 2018. 1
- [35] Vignesh Ramanathan, Congcong Li, Jia Deng, Wei Han, Zhen Li, Kunlong Gu, Yang Song, Samy Bengio, Charles Rosenberg, and Li Fei-Fei. Learning semantic relationships for better action retrieval in images. In *Proceedings of the IEEE conference on computer vision and pattern recognition*, pages 1100–1109, 2015. 1
- [36] Jiawei Ren, Cunjun Yu, Shunan Sheng, Xiao Ma, Haiyu Zhao, Shuai Yi, and Hongsheng Li. Balanced meta-softmax for long-tailed visual recognition. *arXiv preprint arXiv:2007.10740*, 2020. 1, 8
- [37] Shaoqing Ren, Kaiming He, Ross Girshick, and Jian Sun. Faster r-cnn: Towards real-time object detection with region proposal networks. In *Advances in neural information processing systems*, 2015. 5
- [38] Li Shen, Zhouchen Lin, and Qingming Huang. Relay back-propagation for effective learning of deep convolutional neural networks. In Bastian Leibe, Jiri Matas, Nicu Sebe, and Max Welling, editors, *European Conference on Computer Vision ECCV*, 2016. 2, 4
- [39] Abhinav Shrivastava, Abhinav Gupta, and Ross Girshick. Training region-based object detectors with online hard example mining. In *Proceedings of the IEEE Conference on Computer Vision and Pattern Recognition (CVPR)*, June 2016. 13
- [40] Oytun Ulutan, A. S. M. Iftekhhar, and B. S. Manjunath. Vs-gnet: Spatial attention network for detecting human object interactions using graph convolutions. In *2020 IEEE/CVF Conference on Computer Vision and Pattern Recognition, CVPR 2020, Seattle, WA, USA, June 13-19, 2020*, pages 13614–13623. IEEE, 2020. 6
- [41] Petar Veličković, Guillem Cucurull, Arantxa Casanova, Adriana Romero, Pietro Liò, and Yoshua Bengio. Graph attention networks. In *ICLR*, 2018. 5, 8
- [42] Oriol Vinyals, Alexander Toshev, Samy Bengio, and Dumitru Erhan. Show and tell: Lessons learned from the 2015 mscoco image captioning challenge. *IEEE transactions on pattern analysis and machine intelligence*, 39(4):652–663, 2016. 1
- [43] Bo Wan, Desen Zhou, Yongfei Liu, Rongjie Li, and Xuming He. Pose-aware multi-level feature network for human object interaction detection. In *International Conference on Computer Vision, ICCV*, 2019. 1, 2, 6
- [44] Hai Wang, Wei-Shi Zheng, and Yingbiao Ling. Contextual heterogeneous graph network for human-object interaction detection. *CoRR*, abs/2010.10001, 2020. 6
- [45] Tiancai Wang, Rao Muhammad Anwer, Muhammad Haris Khan, Fahad Shahbaz Khan, Yanwei Pang, Ling Shao, and Jorma Laaksonen. Deep contextual attention for human-object interaction detection. In *2019 IEEE/CVF International Conference on Computer Vision, ICCV 2019, Seoul, Korea (South), October 27 - November 2, 2019*, pages 5693–5701. IEEE, 2019. 6
- [46] Tiancai Wang, Tong Yang, Martin Danelljan, Fahad Shahbaz Khan, Xiangyu Zhang, and Jian Sun. Learning human-object interaction detection using interaction points. In *Proceedings of the IEEE/CVF Conference on Computer Vision and Pattern Recognition*, pages 4116–4125, 2020. 2, 6
- [47] Yu-Xiong Wang, Deva Ramanan, and Martial Hebert. Learning to model the tail. In *Advances in Neural Information Processing Systems*, pages 7029–7039, 2017. 2
- [48] Meng Wei, Chun Yuan, Xiaoyu Yue, and Kuo Zhong. Hose-net: Higher order structure embedded network for scene graph generation. *CoRR*, 2020. 6
- [49] Bingjie Xu, Junnan Li, Yongkang Wong, Qi Zhao, and Mohan S Kankanhalli. Interact as you intend: Intention-driven human-object interaction detection. *IEEE Transactions on Multimedia*, 22(6):1423–1432, 2019. 2
- [50] Bingjie Xu, Yongkang Wong, Junnan Li, Qi Zhao, and Mohan S Kankanhalli. Learning to detect human-object interactions with knowledge. In *Proceedings of the IEEE Conference on Computer Vision and Pattern Recognition*, 2019. 2, 4
- [51] Dongming Yang and Yuexian Zou. A graph-based interactive reasoning for human-object interaction detection. In Christian Bessiere, editor, *Proceedings of the Twenty-Ninth International Joint Conference on Artificial Intelligence, IJCAI 2020*. ijcai.org, 2020. 6

- [52] Ting Yao, Yingwei Pan, Yehao Li, and Tao Mei. Exploring visual relationship for image captioning. In *Proceedings of the European conference on computer vision (ECCV)*, pages 684–699, 2018. 1
- [53] Guojun Yin, Lu Sheng, Bin Liu, Nenghai Yu, Xiaogang Wang, Jing Shao, and Chen Change Loy. Zoom-net: Mining deep feature interactions for visual relationship recognition. In *Computer Vision - ECCV 2018 - 15th European Conference, Munich, Germany, September 8-14, 2018, Proceedings, Part III*, 2018. 6
- [54] Cunjun Yu, Xiao Ma, Jiawei Ren, Haiyu Zhao, and Shuai Yi. Spatio-temporal graph transformer networks for pedestrian trajectory prediction. *arXiv preprint arXiv:2005.08514*, 2020. 5
- [55] Ruichi Yu, Ang Li, Vlad I. Morariu, and Larry S. Davis. Visual relationship detection with internal and external linguistic knowledge distillation. In *IEEE International Conference on Computer Vision, ICCV 2017, Venice, Italy, October 22-29, 2017*, 2017. 6, 7
- [56] Yibing Zhan, Jun Yu, Ting Yu, and Dacheng Tao. Multi-task compositional network for visual relationship detection. *International Journal of Computer Vision*, 128(8):2146–2165, 2020. 6, 7
- [57] Ji Zhang, Kevin J. Shih, Ahmed Elgammal, Andrew Tao, and Bryan Catanzaro. Graphical contrastive losses for scene graph parsing. In *IEEE Conference on Computer Vision and Pattern Recognition, CVPR 2019, Long Beach, CA, USA, June 16-20, 2019*, 2019. 3, 5, 6, 7, 8
- [58] Xubin Zhong, Changxing Ding, Xian Qu, and Dacheng Tao. Polysemy deciphering network for robust human-object interaction detection. *CoRR*, 2020. 6, 7, 11
- [59] Hao Zhou, Chongyang Zhang, and Chuanping Hu. Visual relationship detection with relative location mining. In Laurent Amsaleg, Benoit Huet, Martha A. Larson, Guillaume Gravier, Hayley Hung, Chong-Wah Ngo, and Wei Tsang Ooi, editors, *Proceedings of the 27th ACM International Conference on Multimedia, MM 2019, Nice, France, October 21-25, 2019*. ACM, 2019. 3, 5

A. Implementation Details

A.1. Overall Pipeline

The overall pipeline of SABRA consists of three major components: backbone, detector, and VRD classifier. Backbone is a feature extractor for object detection and relationship detection. Detector predicts all potential bounding boxes and produces a set of detections:

$$B = \{(x_1, y_1, x_2, y_2, cls, score)\}, \quad (12)$$

where (x_1, y_1) are the coordinates of the upper left corner, (x_2, y_2) are the coordinates of the bottom right corner, cls is the category of this bounding box, and $score$ is the confidence of this prediction. VRD classifier uses this set of

detections to generate all relationship proposals S and categorize each proposal. In this way, we obtain a set of triplets associated with a $score$ from VRD classifier:

$$T = \{(b_1, b_2, cls, score)\}. \quad (13)$$

A.2. Backbone

To fully compare with other methods, we use several backbone setups in experiments including VGG-16, ResNet50, ResNet50-FPN, ResNet101, and ResNet152. In particular, when we use ResNet50-FPN for both object detection and relationship detection following [14], we use *ResNet50-FPN* to denote this setting. Meanwhile, some other works like [58] use ResNet50-FPN for object detection, but use only ResNet50 for relationship detection. Therefore, we build up this setting named *ResNet50* that a ResNet50 module is shared for both object detection and relationship detection, and an extra FPN is used only for object detection. In addition, FPN is used neither in object detection nor relationship detection process when we use VGG-16, ResNet101, and ResNet152 as the backbone.

Specifically, for V-COCO and HICO-DET datasets, we use ImageNet + MS COCO pre-trained ResNet50, ResNet50-FPN, and ResNet152. For VRD dataset, we respectively use VGG-16 pre-trained on ImageNet, ImageNet + MS COCO, and ImageNet + Visual Genome. We also use ImageNet pre-trained ResNet101 for VRD task.

A.3. VRD Classifier

The overall structure of the VRD classifier is shown in Fig. 2 in the main text. In this section, we will describe the training strategy and inference procedure of our VRD classifier.

Training Strategy VRD classifier receives the detection set B and further divides it into two sets B_{subject} and B_{object} . In HOI task, B_{subject} contains all human bounding boxes and B_{object} contains all bounding boxes from detector. In general VRD task, both B_{subject} and B_{object} contain all detection results. Under this definition, we generate a proposal set S . For each image, we sample 64 relationship proposals from the set S . This hyper-parameter holds across all our model configurations, no matter whether we use BNPS. Moreover, we also keep the ratio of positive proposals as 0.25 for all experiments. Sigmoid activation is used to predict both the confidence of each category and the spatial mask. Correspondingly, binary cross-entropy loss is used for both supervisions.

Inference Procedure For each relationship proposal (b_1, b_2) , we predict the score s_{cls} of each relationship category cls . The final score of triplet (b_1, b_2, cls) is calculated as below:

$$score = s_1 \times s_2 \times s_{cls}, \quad (14)$$

where s_1 and s_2 are the scores of bounding box b_1 and b_2 respectively.

B. Experiment Setup

B.1. Data Preprocessing

For V-COCO, the ground truth detection is obtained from COCO. As some relationships containing invisible objects, we fill the region of the object with the coordinates as the subject. In other words, we generate a ground truth triplet (b_1, b_2, cls) when the object is invisible.

For HICO-DET, we generate ground truth detection from all bounding boxes of triplets. It should be noted that, in HICO-DET, the annotation of each relationship is independent. Therefore, there may exist multiple bounding boxes for a single person or object. To generate a unique bounding box annotation for each instance, we merge those bounding boxes where the IoU values are no less than 0.5.

For general VRD, we have no extra pre-processing.

B.2. Training Procedure

For V-COCO, we first train the object detection on the COCO dataset. Then we freeze the backbone and jointly train the detector and VRD classifier on the corresponding dataset.

For HICO-DET, we first train the object detection on the COCO dataset and then finetune on the detection results from HICO-DET. After that, we jointly train the Detector and VRD classifier with a frozen backbone.

For general VRD, we use ImageNet pre-trained VGG-16 backbone to initialize our model and then train object detection on the general VRD dataset. Finally, we jointly train the detector and VRD classifier with the frozen backbone.

In each training process, we use 16 GPUs (1080TI) and train 25 epochs with the initial learning rate being 0.00125. The learning rate is decreased in the 17th and 23rd epoch with a 0.1 decay rate. When training solely the object detection, each batch contains four different images. For the joint training of detection and relationship detection, each batch contains two different images.

C. Additional Analysis for BNPS

C.1. Other reasons for inaccurate detections

Although inaccurate bounding boxes lead to a large number of easy negative proposals, we cannot simply ignore these detection results. We observe that decreasing the number of top- N detections may have a negative influence on VRD algorithms. Table 4 is a thorough comparison of the top- N detections we keep from the detector and whether

| Detection Top- N | RS | BNPS |
|--------------------|-------|--------------|
| 100 | 51.95 | 54.29 |
| 50 | 52.82 | 54.69 |
| 40 | 52.53 | 54.43 |
| 30 | 53.05 | 54.52 |
| 20 | 52.92 | 53.68 |

Table 4. AP_{role} performance of the different numbers of detections from the detector on the V-COCO test set. We use ResNet50-FPN as our backbone and modify the sampling strategy and selection of the detector’s top- N while keeping others unchanged.

we use BNPS or random sampling (RS) against the model performance. The results suggest that decreasing the number of top- N has no evident improvement in the final performance (Top-50 w/o BNPS V.S. Top-30 w/o BNPS, 52.82 V.S. 53.05). The major reason is that we still need many inaccurate bounding boxes in inference for higher recall values. Besides, we find that our proposed Balanced Negative Proposal Sampling has remarkable improvement no matter which top- N we select. These results strongly prove the effectiveness and robustness of our proposed method.

C.2. Analysis of the improvement

The improvement of BNPS comes from two major sources. Firstly, BNPS reduces the easy negative proposals caused by inaccurate detections; secondly, BNPS balances the difficult negative proposals, considering whether the subject and the object are involved in any triplet from the ground truth. These two parts are both significant and essential, which is partially proven in the ablation study. In this section, we add some extra quantitative and qualitative results.

We include an additional experiment to test if the performance improvement of SABRA comes only from the increase in the number of difficult negative proposals $S_{neg}^{3:5}$. We compare a BNPS-3cls variant, BNPS-3cls-HN with BNPS. In the original BNPS-3cls, we use a sample rate [0.25, 0.25, 0.25] for S_{neg}^1 , S_{neg}^2 and $S_{neg}^{3:5}$. However, in BNPS, each class receives a sample rate of 0.15, which gives a 0.45 sample rate for the negative classes $S_{neg}^{3:5}$. We design BNPS-3cls-HN such that it assigns the same sample rate to the hard negative classes, [0.15, 0.15, 0.45] for S_{neg}^1 , S_{neg}^2 and $S_{neg}^{3:5}$. We train both models on V-COCO and report the results briefly here: BNPS-3cls-HN gives 54.20 AP_{role} while SABRA achieves 54.69. This suggests that the improvement from BNPS-3cls to SABRA is not simply because of the increased sample rate of hard negative proposals. The balance among $S_{neg}^{3:5}$ also plays a critical role in this improvement.

We also visualize the number of negative predictions of each negative type in Fig. 5. We observe that: (1) the total number of false positives in low-frequency difficult classes,

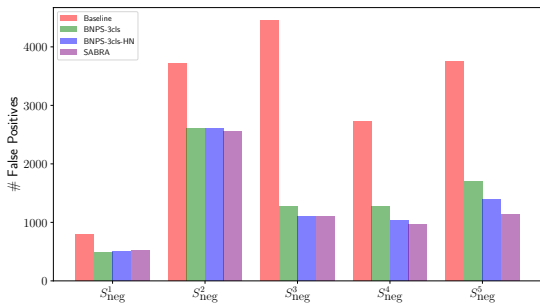


Figure 5. Qualitative analysis of different sampling strategies.

$S_{neg}^{3:5}$, of SABRA is lower than BNPS-3cls because we increase the total ratio of difficult negative proposals. (2) the reduction ratio of S_{neg}^5 is higher than that of S_{neg}^4 . Meanwhile, the reduction ratio of S_{neg}^4 is higher than that of S_{neg}^3 , which suggests that our balance among S_{neg}^3 , S_{neg}^4 , S_{neg}^5 clearly improves the ability to identify the negative proposals, especially on the difficult proposals.

C.3. BNPS compared with other sampling methods

We have proved the rationality and effectiveness of our proposed BNPS in sampling ideal relationship pairs among a vast number of proposals. To further examine the superiority of BNPS, we implement several alternative sampling methods including *online hard example mining (OHEM)* [39] and *focal loss* [26] and compare their capacities.

OHEM was first proposed in the object detection area and it prefers to sample harder examples than easier ones [39]. Typically, for a mini-batch of samples, only the top- k most difficult proposals, i.e. proposals with top- k highest loss values, will contribute to model optimization. In practice, the mini-batch is constructed to enforce a 1:3 ratio between positives and negatives, i.e. proposals in S_{pos} and S_{neg} , to help ensure each mini-batch has enough positives. Since positive proposals are usually insufficient, we only apply OHEM on S_{neg} to ensure this claim. We set mini-batch size $B \in \{48, 64, 96\}$ in our experiment.

The focal loss modifies the standard cross-entropy loss to dynamically down-weight the contribution of easy examples:

$$\begin{aligned}
 \text{FL}(p_t) &= -\alpha(1-p_t)^\gamma \log(p_t), \\
 p_t &= \begin{cases} p & \text{if } y = 1 \\ 1-p & \text{otherwise.} \end{cases} \quad (15)
 \end{aligned}$$

In the above $y \in \{\pm 1\}$ specifies the ground-truth class and $p \in [0, 1]$ is the model’s estimated probability for the class with label $y = 1$. α and γ are the balance coefficient and the tunable focusing parameter respectively. In our experiment, we use $\alpha = 0.25$ with $\gamma \in \{1, 2\}$.

Besides the above methods, Random Sampling and

BNPS are also implemented as relationship pair sampling methods for comparison. We train models using these methods on V-COCO and keep all other settings consistent with setups in Section B. Additionally, we assign $N = 50$ for top- N detections.

As results shown in Table 5, we observe that BNPS achieves the best performance, which reconfirms its superiority. Meanwhile, focal loss and OHEM in all settings behave worse than the basic random sampling method, which draws our attention. Focal loss and OHEM both emphasize the importance of samples with high loss values. However, in the scenario of relationship detection, these methods may focus too much on the hard samples and overlook the role of easy ones. Compared with them, our proposed BNPS uses the predefined sample classification method and pay equal attention to 5 classes of negative proposals, which makes our sampling strategy more robust towards the complicated distribution of samples in this scenario and less likely to be influenced by outliers.

| Method | Setup | AP_{role} |
|------------|--------------|--------------------|
| RS | - | 52.82 |
| | $B = 48$ | 45.81 |
| | $B = 96$ | 45.73 |
| Focal Loss | $\gamma = 1$ | 52.55 |
| | $\gamma = 2$ | 51.10 |
| BNPS | - | 54.69 |

Table 5. Performance of the different relationship pair sampling methods. We use ResNet50-FPN as our backbone and modify the sampling strategy while keeping others unchanged.